Metallurgical Characteristics of Pulsed, High Pressure Weldments

Welding is successfully carried out on similar and dissimilar, ferrous and nonferrous alloy couples, producing optimum metallurgical features and minimal microstructural damage

BY M. P. BERARDI, J. ZOTOS AND S. WEISS

ABSTRACT. Pulsed, high pressure weldments have been created by the hydro-dynamic welding (HDW) process between similar and dissimilar, ferrous and non-ferrous alloy couples. The joints produced had optimum metallurgical features and minimal microstructural damage in either the parent alloys or in the welded sections. The significant metallographic, micro-hardness and electron beam microprobe analysis results suggest the metallurgical joining mechanism for HDW is as follows:

1. The short heating cycle results in a thin oxide skin buildup at the interface.
2. The localized pressure wave produced by the "self pinch" phenomenon seals the interface, and reduction of the metal oxide commences in the joining region.
3. The lagging thermal spike created by the pressure pulse destroys the interfacial oxide and further promotes diffusion across the boundary, thus creating the HDW joint.

Introduction

Metallurgical joining has been accomplished between similar and dissimilar metals and alloys through the use of heat and localized pressure transmitted through a common weld head. The process and equipment have been developed and tested during the past six years and is called hydro-dynamic welding (HDW).* HDW is a radical departure from present processes in that it requires no weld metal and offers the advantages of speed, reproducibility, and automatic operation, while producing an optimum joint.[1-7]

Figure 1 illustrates an HDW console, which coupled with a 10,000 hz motor generator set, provides a metal joiner that can preheat, weld, and postheat treat similar and dissimilar metals and alloys. Figure 2 shows a work piece positioned in the weld head. The entire welding process is completely programmable with up to three variable heat-pressure cycles possible, using an automatic, single button operation.

Since the process and equipment are relatively new, their full capabilities and limitations have not been completely determined. To date, the process has metallurgically joined similar and dissimilar materials with the following configuration specifications:

1. Area overlapping and/or butt-type interface.
2. The area to be joined must be circumferentially continuous.
3. The configuration size is dictated by the available power supply.

These restrictions are based on the state-of-the-art development of HDW and not on the physics of the process. In addition, since the basic process is independent of any environmental interaction, it can be utilized for joining metals and alloys that either normally require very specialized and sophisticated equipment or perhaps cannot be effectively joined by other methods.

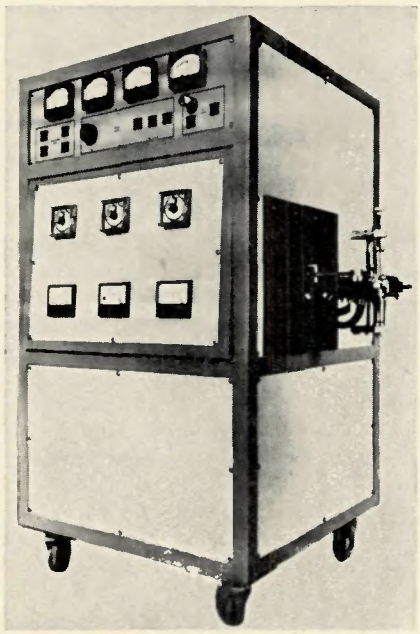

Fig. 1—Hydro-dynamic welding console with special welding head (at right)

Preliminary Metallurgical Considerations

Since HDW joining is accomplished in seconds, the process is quite non-equilibrium with respect to the predicted phase diagram response of the alloy systems involved. The times, temperatures, compositions, phase transformations, invariant reactions, and other data normally used, must therefore be examined with an emphasis on meta-stability. The projection of equilibrium data to non-equilibrium conditions helps one to predict and understand these highly meta-stable, pulsed, high pressure weldments obtained using this process.

When similar materials are to be joined utilizing HDW, a study of the equilibrium phase diagram for the metal or alloy is conducted. In addition, the thermodynamic stability of any oxides present on the surface of those metals or alloys are examined to evaluate whether the oxides can be destroyed during the joining cycle.

It is also necessary to determine the initial melting temperature, (i.e., temperature of the solidus) so that the heating cycle preceding the pressure pulse will not melt the material. With such prior knowledge, joining parame-

* Hydro-dynamic welding is referred to throughout this paper as HDW for purposes of reader convenience.

M. P. BERARDI is Product Manager, Industrial Magnetics, Inc., Canton, Mass.; J. ZOTOS is Associate Professor, Northeastern University, Boston, Mass., and S. WEISS is Associate Professor, University of Wisconsin, Milwaukee, Wisc.

Paper presented at the AWS 51st Annual Meeting held in Cleveland, Ohio, during June 8-12, 1970.

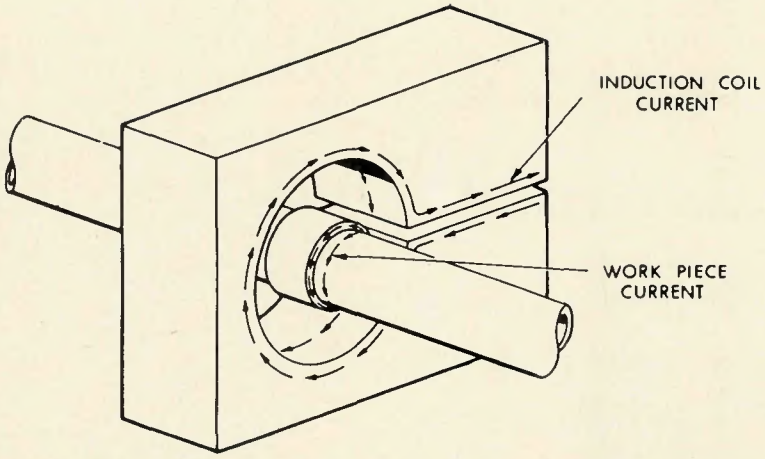

Fig. 2—Schematic showing current flow during welding cycle in welding head and work piece

ters can be predetermined to some extent, thus decreasing to a minimum the trial-and-error procedures necessary to effect an acceptable joint.

In attempts to join dissimilar metals or alloys, the same procedure is followed, i.e., analyses of phase equilibrium data and thermodynamic information are made. The main objective of an in-depth physical metallurgy investigation is to determine what potential interfacial intermetallic compounds, solid solutions, and invariant reactions might be present between the dissimilar alloy couple after joining.

If any detrimental compounds are present in the equilibrium phase diagrams, one can expect to find them in the HDW joined interface. However, certain steps can be taken to minimize and/or eliminate the formation of these detrimental phases. These steps include but are not limited to:

1. Redesigning the joint configuration.

2. Adjusting the weld parameters to minimize heat inputs.

Table 1—Electron Beam Microprobe Analysis of HDW Joined 1008 Plain Carbon Steel Couple

Area of test	Composition, wt-%[a] Fe	Mn	Si	S
Interface	99	0.4	0.12	0.2
Interface	99	0.8	0.23	0.2
Interface	99	0.7	0.17	<0.1
Interface	99	0.7	0.17	<0.1
Interface	99	0.5	0.12	<0.1
Adjacent to bond	99	0.3	0.06	<0.1
Adjacent to bond	99	0.6	0.12	<0.1
Adjacent to bond	99	0.6	0.17	<0.1
Adjacent to bond	99	0.8	0.12	0.1
Analytical precision, %	±1-2	±0.1	±0.05	±0.1

3. Surface coating the dissimilar coupling with a material compatible to both members.

This evaluation further tends to reduce the trial-and-error experimental time required to effect metallurgical joining between vastly dissimilar metals and alloys.

Experimental Procedure

This investigation evaluated the metallurgical characteristics of the weldments produced by the HDW process between both similar and dissimilar alloy components. The joint interfaces resembled both straight socket and combined butt-socket types of geometric configurations.

The similar alloy couples evaluated included both ferrous and non-ferrous metal systems and were as follows:

1. 1008 plain carbon steel.
2. 1020 plain carbon steel.
3. 321 stainless steel.
4. Ti-6A1-4V titanium alloy.
5. 6061 aluminum alloy.

The dissimilar alloy couples included both ferrous and non-ferrous metal systems and were as follows:

1. Sintered iron to 4130 alloy steel.
2. 1080 eutectoid plain carbon steel to ductile cast iron.
3. Copper to 1100 aluminum.
4. Copper to 1100 aluminum with a zincate coating.

Both macroscopic and microscopic metallographic techniques were employed to evaluate the nature of each joined region. The macro cross section of an acceptable joint between similar alloys showed the disappearance of the prior interface in the welded region. In dissimilar couples, on the other hand, a chemical variation indicated the presence of a prior interface. The microscopic analyses of the joined sections between both similar and dissimilar alloys showed grains growing across the entire joined regions along with indications of

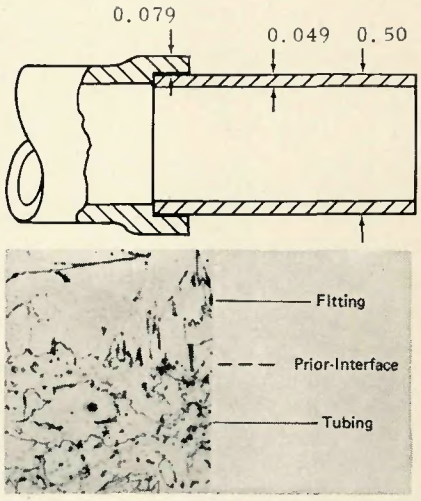

Fig. 3—Hydro-dynamic welding of 1008 plain carbon steel. Top—joint configuration. Bottom—weld section; 2% nital etch; X100 (reduced 32% on reproduction)

chemical gradients.

In some instances, microhardness profiles were obtained across the joined sections to enhance the metallurgical analysis.

Alloy couples of metallurgical and industrial interest were electron beam microanalyzed to further study interfacial metallurgical mechanisms involved during the joining of both the similar and dissimilar alloy couples.

Results and Discussion

The first similar, ferrous alloy couple examined in this investigation was a 1008 plain carbon steel; the joint configuration was of the straight socket type. Figure 3 shows that, after subjecting the parts to the HDW process, prior interfaces were eliminated in the joined region as evidenced by the presence of random ferrite and pearlite grains across the entire welded section and the absence of a continuous oxide interface. In addition,

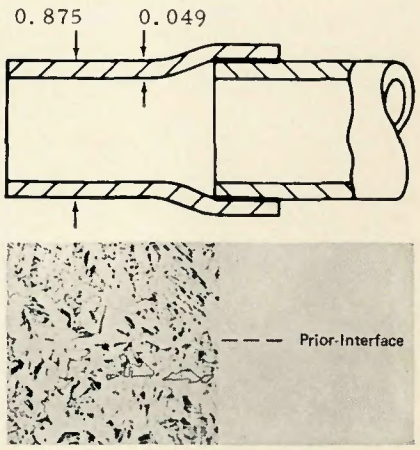

Fig. 4—Hydro-dynamic welding of 1020 plain carbon steel. Top—joint configuration. Bottom—weld section; 1% nital etch; X100 (reduced 32% on reproduction)

decarburization, porosity or shrinkage were not present within the joint vicinity.

Table 1 summarizes the qualitative and quantitative analyses conducted for iron (Fe), manganese (Mn), silicon (Si), and sulfur (S). For this work, an electron beam microprobe was used[8] in scans encompassing the weld zone and unaffected base metal. The only variation in solid solution matrix chemistry observed was in the manganese concentration which ranged between 0.3 and 0.8 wt-%. These composition variations can be attributed to normal chemistry gradients in the tubing base metal.

Figure 4 illustrates the various features of the 1020 plain carbon steel couple in the straight socket configurations. The prior interface was eliminated in the joined region as evidenced by the presence of ferrite and pearlite grains across the entire welded section.

Table 2 summarizes the microprobe analyses for iron, managanese, and carbon[8] in the joined section of the 1020 steel alloy. The ferrite phase contained 0.4 wt-% carbon and 0.7 wt-% manganese, while the pearlite regions had 1 to 2 wt-% carbon and approximately 0.7 wt-% manganese. A slight manganese depletion was evident at one interface point where the

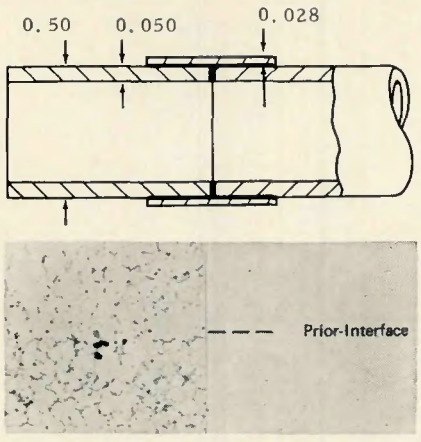

Fig. 5—Hydro-dynamic welding of Type 321 stainless steel. Top—joint configuration. Bottom—weld section; 50% water and 50% nitric acid electrolytic etch. X100 (reduced 32% on reproduction)

composition dropped to about 0.5 wt-%. This slight variation was attributed to normal gradients in this tube material.

Figure 5 shows the characteristics of the joined Type 321 stainless steel couple in the straight socket configuration. The prior interface has been eliminated and excellent metallurgical joining achieved.

Table 3 summarizes the results of the microprobe analyses for iron, chromium, manganese, titanium, and nickel in and around the bonded section of the Type 321 stainless steel alloy. The joined region exhibits a grain boundary phase in the vicinity of the weld. The composition of the matrix phase in the joined region did not vary significantly from that in the unaffected regions of this stainless steel couple. The grain boundary sigma phase has less iron and nickel content and more chromium, manganese, and titanium content compared to the base material.

The angular phase found in the Type 321 stainless steel base metal was found to be rich in both titanium and carbon, i.e., it was titanium carbide.

Figure 6 illustrates the features of the titanium alloy (Ti-6Al-4V) tube couple using a modified butt-socket configuration. While most of the ferrous alloys were joined in air, the titanium specimens were welded in an argon atmosphere. Metallurgical joining was again confirmed by the presence of grains across the entire prior interface.

The electron beam microprobe analyses of the Ti-6Al-4V alloy indicated that a vanadium-rich and aluminum-poor area, approximately 50μ wide, was present at the prior interface. The vanadium content in this region increased from 3.7 to 4.9 wt-%, while the aluminum dropped from 5.5 to 4.5 wt-%; and no titanium variation was detected in this area. No significant variation in the concentration distribution of the three elements was found outside the vanadium-rich, aluminum-poor zone.

Table 4 summarizes the microhardness probe results taken across the joined interface of the Ti-6Al-4V titanium alloy. The mean diamond pyramid hardness (DPH) numbers in the weld zone ranged from 346 to 349. Adjacent to this region they were 349 to 350 as contrasted to values of

Table 2—Electron Beam Microprobe Analysis of HDW Joined 1020 Plain Carbon Steel Couple

Area of test	Composition, wt-%[8] Fe	Mn	C
Interface: Ferrite	97.8	0.59	<0.4
Pearlite	97.5	0.71	1.2
Interface: Ferrite	98.7	0.50	<0.4
Pearlite	96.5	0.52	1.7
Interface: Ferrite	98.7	0.61	0.5
Pearlite	97.8	0.71	2 2
Interface: Ferrite	99.3	0.72	<0.4
Pearlite	96.7	0.70	1.0
Adjacent to bond: Ferrite	99.5	0.76	<0.4
Pearlite	98.7	0.80	1.1
Adjacent to bond: Ferrite	97.8	0.63	0.7
Pearlite	96.8	0.71	1.4
Analytical precision, %	±1–2	±0.07	±0.4

Table 3—Electron Beam Microprobe Analysis of HDW Joined Type 321 Stainless Steel Couple

Area of test	Composition, wt-%[8] Fe	Cr	Mn	Ti	Ni
Interface matrix	66.2	15.6	1.3	0.29	11.7
Interface matrix	67.0	15.1	1.7	0.53	11.6
Interface matrix	64.8	15.1	1.8	0.61	11.0
Interface matrix	64.0	15.2	1.4	0.35	11.7
Adjacent matrix	67.5	15.8	1.3	0.48	11.8
Adjacent matrix	67.0	14.8	1.2	0.35	12.1
Unaffected matrix	67.2	15.1	1.6	0.55	11.8
Interface grain boundary phase	63.0	21.4	1.8	0.79	9.4
Adjacent matrix grain boundary phase	63.0	22.4	1.7	0.94	8.6
Adjacent matrix grain boundary phase	63.7	22.0	1.4	0.64	8.1
Angular phase in unaffected matrix	29.0	3.7	0.4	0.56	7.4
Analytical precision, %	±1–2	±0.3	±0.1	±0.02	±0.1

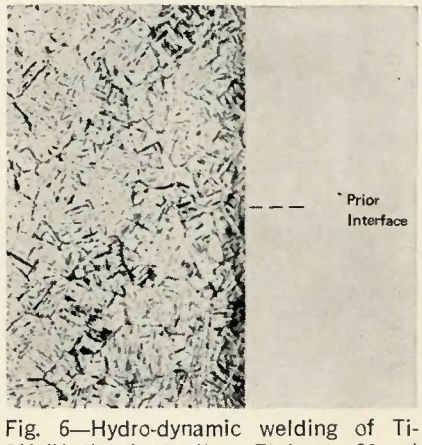

Fig. 6—Hydro-dynamic welding of Ti-6Al-4V titanium alloy. Etchant: 20 ml hydrofluoric acid; 20 ml nitric acid; 60 ml glycerol. X100 (reduced 35% on reproduction)

Table 4—Diamond Pyramid Hardness (DPH) Data for HDW Joined Ti-6Al-4V Titanium Alloy

Probe location	Probe direction	Diamond pyramid hardness (DPH) numbers High	Low	Mean
As-received material	Longitudinal	375	271	360
	Transverse	373	355	361
Unaffected zone of HDW joined material	Longitudinal	402	342	371
	Transverse	389	315	349
Weld zone	Longitudinal	402	239	344
	Transverse	389	315	349

360 to 361 in the as-received material. Thus, the hardness of this alloy was not significantly changed by the joining process. These hardness results corroborate with the microprobe findings; i.e., no major chemical change was experienced beyond the 50 micron wide, vanadium-rich and aluminum-poor, interfacial phase.

Figure 7 shows the photomicrographs of the as-received and joined sections of a 6061 aluminum allow whose interface configuration was the straight socket type. The female, filler port section was part of a bomblet half shell, while the male was a filling plug made from fine grained plate stock. Metallurgical joining was achieved as evidenced by the presence of new grains across the prior interface. The joint also exhibited grain growth adjacent to the prior interface. The presence of the fine grained zone was attributed to rapid resolidification of some superficial incipient melting experienced during joining.

The joined sections of the aluminum alloy couple also proved to be leak-tight when subjected to a helium leak rate test of 1.1×10^{-10} standard cc/sec.

Figure 8 shows the characteristics of a sintered iron to 4130 alloy steel tube couple joint in the socket configuration. The photomicrograph again shows the disappearance of the prior interface. This was confirmed by the presence of new grains in the welded region. In addition, the pressed and sintered compact has been considerably densified in the vicinity of the weld region as illustrated by a qualitative comparison of the before and after microstructures.

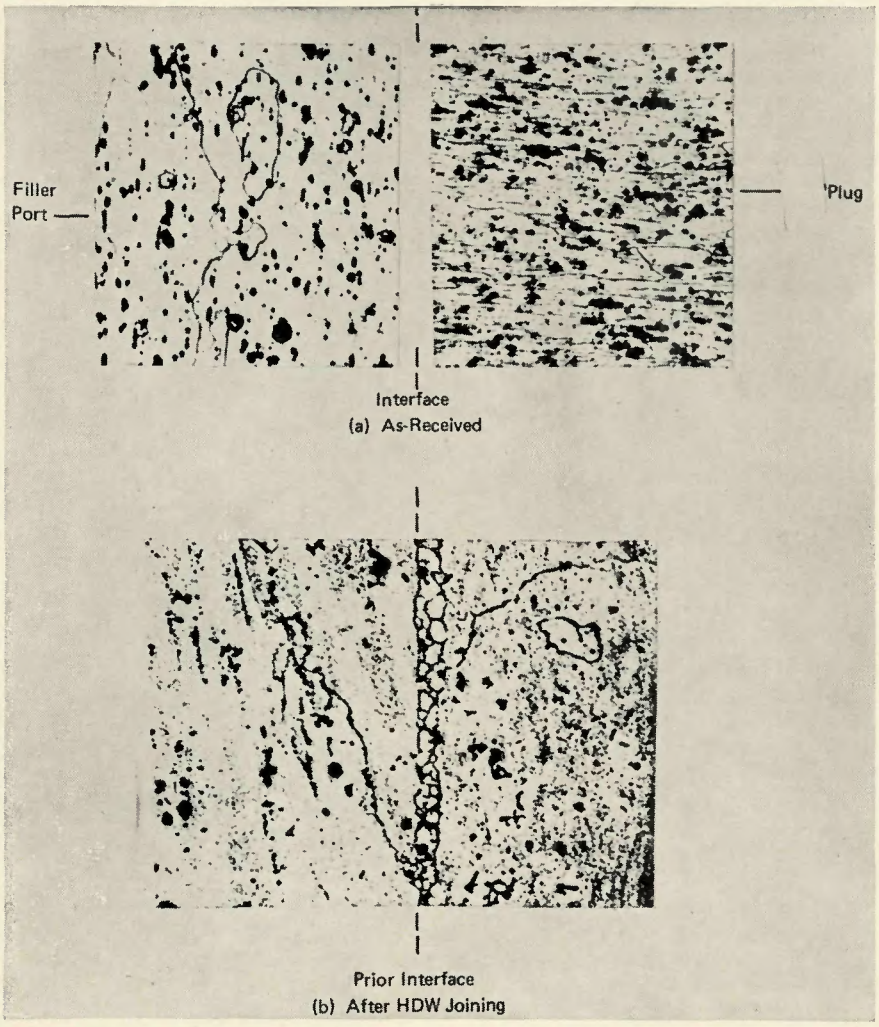

Fig. 7—Photomicrographs of as-received and HDW joined 6061 aluminum alloy. Etchant: 20 ml nitric acid, 20 ml hydrofluoric acid; 60 ml glycerol. X100 (reduced 20% on reproduction)

Results of recent investigations[7] showed that gray, malleable, and nodular cast iron alloys can be joined to plain carbon steel alloys, using this process. The joined sections have optimum metallurgical features and no apparent major microstructural damage in either the base metal cast iron or in the transition zone between the steel and cast irons.

Figure 9 further illustrates these facts, showing the features of a joint between a ductile cast iron component and a eutectoid, plain carbon steel. The prior interface was eliminated as evidenced by the presence of ferrite and pearlite grains across the entire interface. In addition, a carbon gradient was present in the transition zone between the base metal alloys, while the carbon nodules remained intact, even those located at the prior interface. This indicated that joining has taken place without any fusion and accompanying dissolution of carbon.

A microhardness probe of the welded couple revealed some microstructural changes took place adjacent to the joined interface in both alloys. These changes were attributed to the high hardenability of the materials in relation to the rapid cooling cycle following the weld pulse. A postheat treatment consisting of austenitizing at 1650° F for 2 hr, oil quenching, and tempering at 1300° F for 1 hr removed the solid state, metastable phases and restored acceptable hardness levels in the base metals.

Table 5 summarizes the results obtained during the microhardness surveys. The as-received, ductile cast iron has a R_b hardness, which ranged from 83 to 89, while the original R_b hardness of the eutectoid steel ranged from 88 to 95. After joining and without any postheat treatment, the R_c hardness of the cast iron ranged from 43 to 60. The hardness of the steel ranged from R_c 26 to 45; and the R_c hardness at the prior interface was 45. The solid state, metastable phases present in the as-joined alloy couple were eliminated after postheat treatment. This was evidenced by the hardnesses of the cast iron and steel, which were reduced to ranges of R_b 92 to R_c 28 and R_b 92 to R_c 26, respectively. The hardness at the prior interface

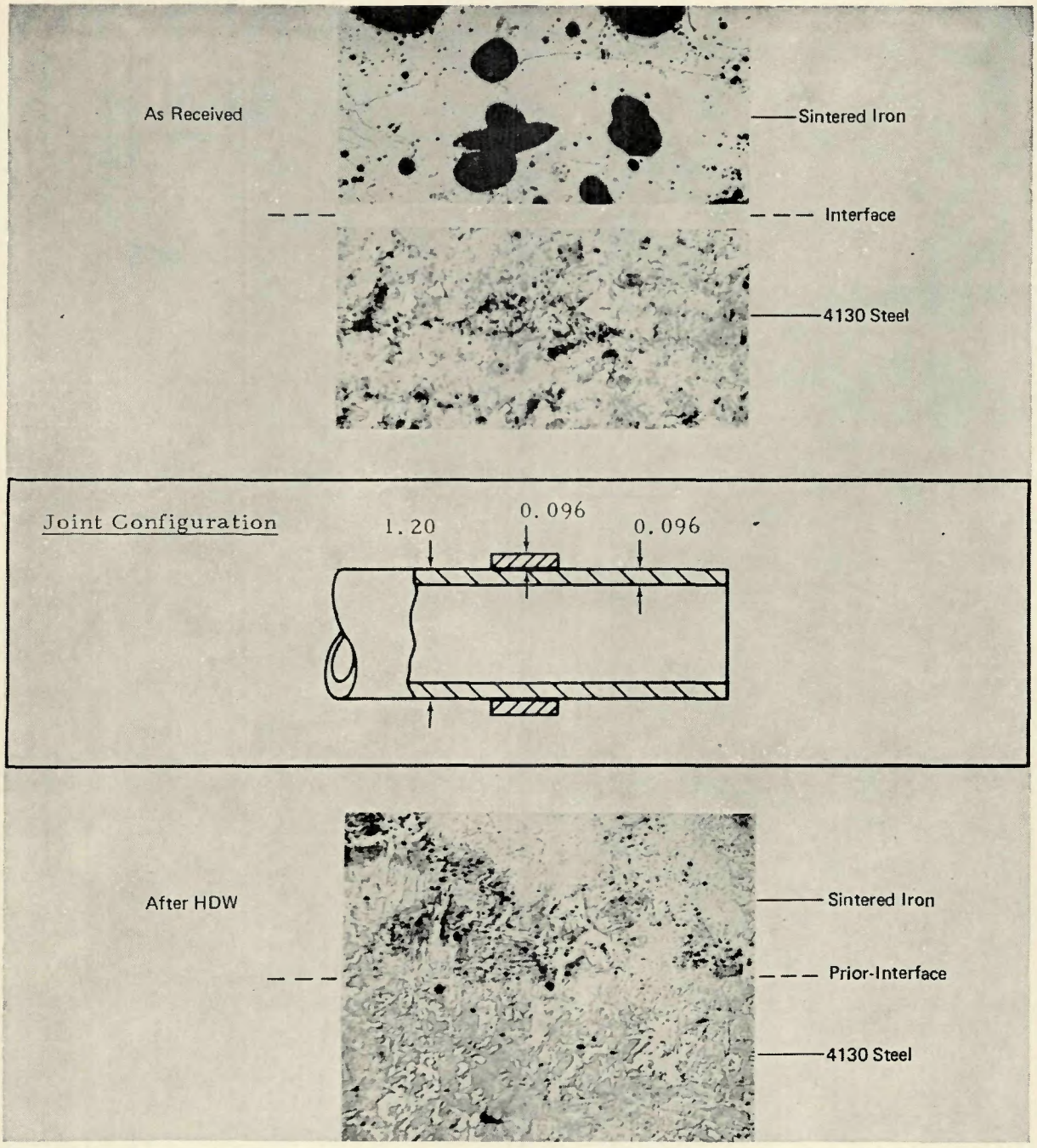

Fig. 8—Hydro-dynamic welding of sintered iron to 4130 steel alloy tubing. Etchant: 2% nital. X60 (reduced 11% on reproduction)

was only R_b 93, i.e., about the mean level of the as-received alloy.

Figure 10 presents a photomicrograph of the joined configuration shown after postheat treatment. It can be seen that a high integrity metallurgical joint exists with no solid state, metastable phase transformations remaining. In addition, retention of the spheroidal nodules at the interface provided dramatic evidence that the joining occurred without gross melting.

Figure 11 shows the features of a metallurgical joint between another nodular cast iron component and a 1020 plain carbon steel tube using a socket configuration. Note that the prior interface was again eliminated as evidenced by the presence of ferrite and pearlite grains across the entire joined section.

Table 6 summarizes the electron beam microprobe analyses for manganese, silicon, carbon, oxygen, and iron in the joined and matrix areas. The matrix areas were located in both the nodular cast iron and steel alloys and in the joined area around the prior interface.

There was no evidence of free precipitates (i.e., procutectoid phase) in the joined area. A small amount of manganese and silicon segregated in the matrix phase of the nodular alloy, and some silicon diffused about 10 μ into the steel matrix. However, the chemical gradients which occurred were not significant and did not affect the integrity of the joint. In addition, since the matrix contained less than 0.5 wt-% carbon, it was identified as ferrite and not iron carbide; i.e., no typical, metastable, white cast iron structure was evident in the interfacial regions of this joint.

Figure 12 illustrates the microstructure of an 1100 aluminum alloy tube joined to a copper tube without any intermediate coatings present. Metallurgical joining was obtained. However, as predicted from the copper-aluminum phase diagram (projected to non-equilibrium), several interme-

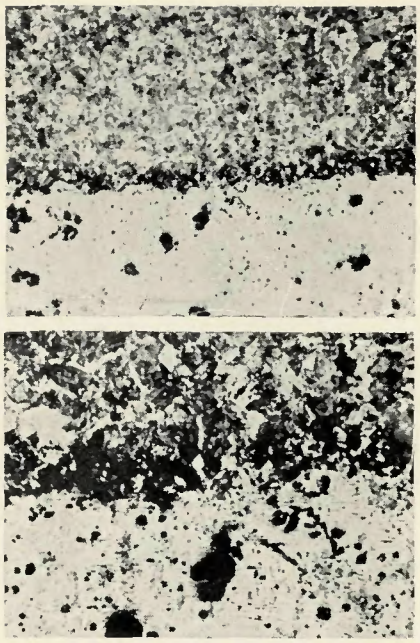

Fig. 9—Hydro-dynamic welding of ductile cast iron to eutectoid steel before heat treatment. Etchant: 2% nital. Top—X47; bottom—X100 (reduced 48% on reproduction)

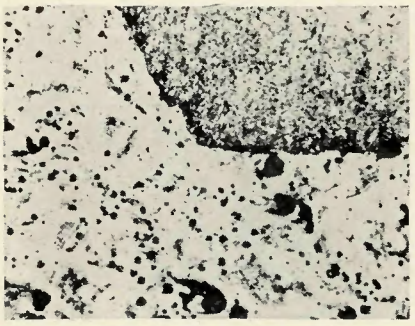

Fig. 10—Hydro-dynamic welding of ductile cast iron to eutectoid steel after heat treatment. Etchant: 2% nital. X100 (reduced 50% on reproduction)

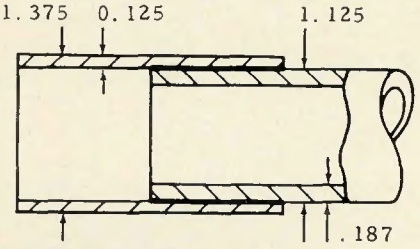

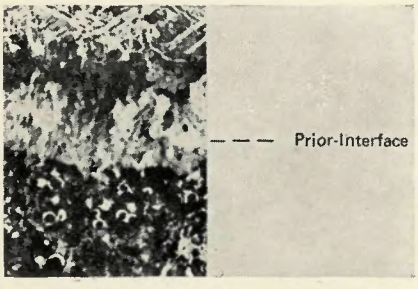

Fig. 11—Hydro-dynamic welding of 1020 plain carbon steel to nodular cast iron. Top—joint configuration. Bottom—weld section; picral etchant; X100 (reduced 28% on reproduction)

Table 5—Microhardness Profile[a] of HDW Joined Steel Rod to Ductile Cast Iron Component

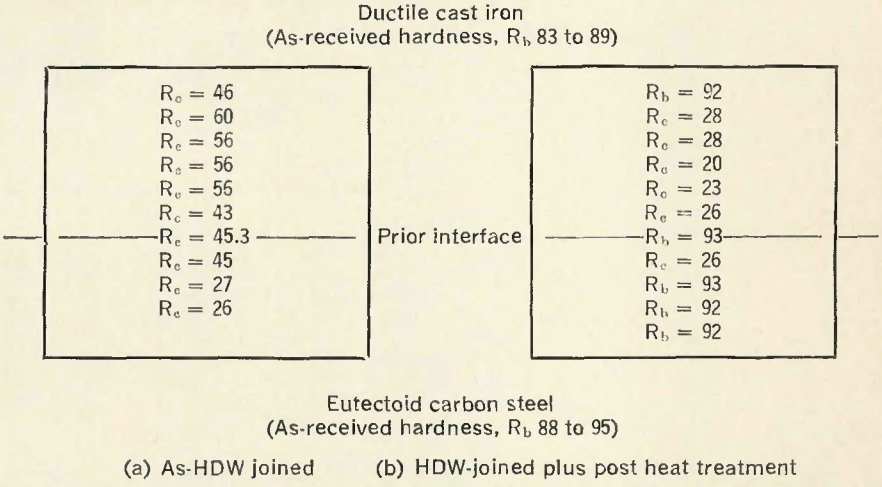

(a) As-HDW joined (b) HDW-joined plus post heat treatment

[a] R_b and R_c hardness numbers are obtained from conversion of DPH data originally obtained from microhardness probes.

tallic compounds were produced at the interface between the two tube materials.

Table 7 summarizes the microhardness probe analyses taken across the joined interface of the copper to 1100 aluminum alloy without any coating. In going from the aluminum alloy towards the copper, both the DPH numbers and chemical analyses identify the presence of the following two terminal solid solutions (aluminum-rich adjacent to the Al, and copper-rich adjacent to the Cu), a very fine eutectic zone, and two discontinuous, extremely thin bands of intermetallic compounds ($CuAl_2$ and CuAl). This gradient of structures was about 0.008 in. thick.

Figure 13 shows the microstructure of a copper tube joined to a zincated, 1100 aluminum alloy tube. Metallurgical joining was again achieved, and the presence of zinc aided in reducing the thickness of the interfacial zone to about 0.0035 in.

Table 8 summarizes the microhardness and microprobe analyses taken across the joined interface of this copper-aluminum couple with the zincate coating. The same phases identified in the previous copper-aluminum transition zone are also present in this specimen's interfacial region along with the presence of some zinc in the eutectic and matrix phases. These results again verify the prediction of the copper-aluminum phase diagram. They also indicate that zincating reduces the thickness of the transition zone. The entire zincate coating was dissolved as a separate phase and no additional layers appeared in the interfacial region.

Proposed HDW Metallurgical Joining Mechanism

The metallographic and electron beam microanalysis results obtained during this investigation provided a basis for describing the HDW joining mechanism.

Since joining is achieved across a common interface using both induc-

Table 6—Electron Beam Microprobe Analysis of HDW Joined 1020 Plain Carbon Steel to Nodular Cast Iron

Area of test	Composition, wt-%[a] Mn	Si	C	O	Fe
Normal nodular cast iron matrix	0.95	2.4	<0.5	<0.3	96.7
60 μ from prior interface	0.88	1.8	<0.5	<0.3	96.9
40 μ from prior interface	1.17	1.9	<0.5	<0.3	95.6
20 μ from prior interface	1.12	1.9	<0.5	<0.3	96.7
10 μ from prior interface	1.16	2.1	<0.5	<0.3	96.7
Prior interface	1.35	1.2	<0.5	<0.3	97.8
10 μ from prior interface	0.63	0.22	<0.5	<0.3	98.2
20 μ from prior interface	0.63	0.10	<0.5	<0.3	99.3
40 μ from prior interface	0.63	0.12	<0.5	<0.3	99.3
60 μ from prior interface	0.66	0.13	<0.5	<0.3	99.3
Normal steel matrix	0.69	0.12	<0.5	<0.3	99.3
Analytical precision, %	±0.04	±0.2-C.I. ±0.04-St.	±0.5	±0.3	± 1.0

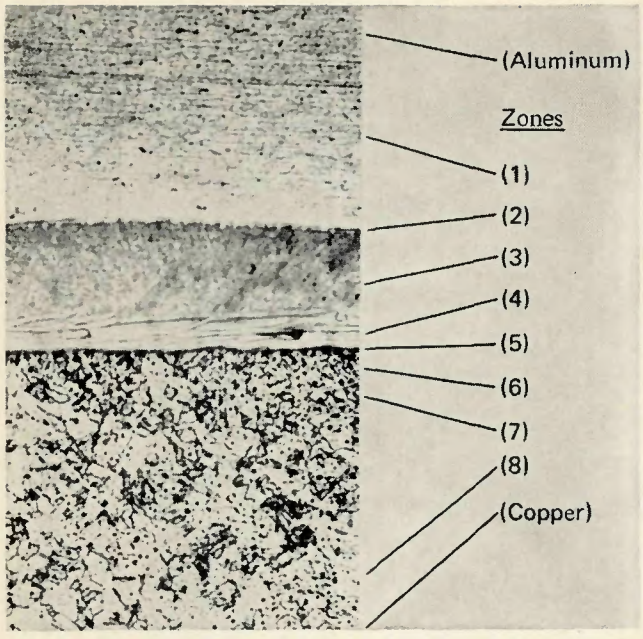

Fig. 12—Hydro-dynamic welding of copper to 1100 aluminum with no coating. Etchant: 20 ml ammonium hydroxide; 10 ml hydrogen peroxide (3%); 30 ml water. X100

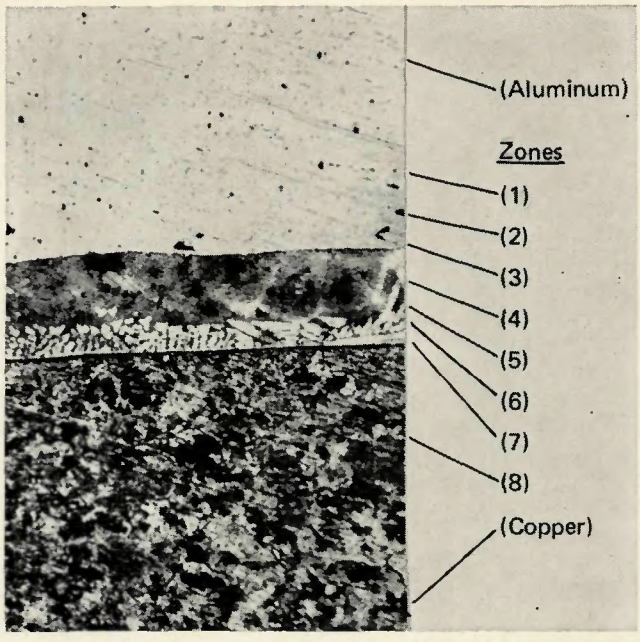

Fig. 13—Hydro-dynamic welding of copper to 1100 aluminum with zincate coating. Etchant: 20 ml ammonium hydroxide; 10 ml hydrogen peroxide; 30 ml water. X100

tion heat and localized pressure, it is first necessary to determine the contribution of these two forms of energy during welding.

The initial heating cycle attempts to raise the temperature of the common interface of the joint to within 100° to 200° of the ambient melting point. During this heating phase, a thin oxide skin occurs due to the relatively short time at high temperatures by the following reaction:

$$M(s) + {}^1/_2O_2(g) = MO(s) \qquad (1)$$

In addition, the diffusivity of the elements in alloy M increases exponentially in accordance with the Arrhenius equation.

Thermodynamically and kinetically, the increased rate of oxidation of alloy M at elevated temperatures is offset by the decreased stability of typical metal oxides at high temperatures. Consequently, oxides tend to disassociate at elevated temperatures due to marked decreases in magnitude of their negative standard free energy of formation.

The localized pressure wave concentrated at the common interface has a two-fold effect; namely:

1. The "self-pinch" phenomenon seals the entire weld section from further interaction with the air environment in the vicinity of the joint.

2. A thermal spike, which lags behind the force of the pulse, is concentrated at the weld interface and superheats the alloy and oxide. This superheat further promotes the destruction of the oxide, and joining is accomplished without the formation of significant melting effects.

Table 7—Microhardness and Microprobe Analyses of HDW Joined Copper to 1100 Aluminum with no Coating

Positions (see Fig. 12)	Diamond pyramid hardness (DPH) numbers	Composition, wt-%[9] Al	Cu	Remarks
(1)	27	—	—	Unaffected 1100 aluminum alloy
(2)	74	99.6±1–2	0.4±0.1	Dendritic zone (i.e., Al-Cu solid solution surrounded by eutectic)
(3)	213	63.6±1–2	37.7±1–2	Very fine, Al-Cu eutectic
(4)	548	42.0±1–2	57.3±1–2	$CuAl_2$ intermetallic compound
(5)	—	35 ±1–2	65 ±1–2	Could be CuAl intermetallic compound[a]
(6)	—	0.7±0.1	99.0±1–2	Cu-Al solid solution
(7)	—	0.5±0.1	99.0±1–2	Cu-Al solid solution
(8)	44	—	—	Unaffected copper

[a] Too small for discrete analysis; therefore, data include excitation of adjacent areas.

Table 8—Microhardness and Microprobe Analyses of HDW Joined Copper to 1100 Aluminum with Zincate Coating

Positions (see Fig. 13)	Diamond pyramid hardness (DPH) numbers	Composition, wt-%[9] Al	Cu	Zn	Remarks
(1)	26	—	—	—	Unaffected 1100 aluminum alloy
(2)	—	100 ±1–2	0.06±0.03	<0.04	Al-Cu solid solution
(3)	—	100 ±1–2	0.17±0.05	<0.04	Al-Cu solid solution
(4)	218	67.3 ±1–2	33.4 ±1–2	<0.1	Very fine, Al-Cu eutectic
(5)	218	68.5 ±1–2	32.6 ±1–2	0.14±0.07	Very fine, Al-Cu eutectic
(6)	380	45.0 ±1–2	45.2 ±1–2	<0.1	$CuAl_2$ intermetallic compound
(7)	—	35.0 ±1–2	66.0 ±1–2	0.10±0.06	CuAl intermetallic compound[a]
(8)	45	<0.01±0.01	100 ±1–2	<0.1	Unaffected copper

[a] Too small for discrete analysis; therefore, data include excitation of adjacent areas.

For most of the alloy systems normally employed for welding, the application of high pressures has a tendency to increase the solidus temperature. Consequently, since the value of the pressure pulse is estimated to be orders of magnitude greater than ambient (of the order of 50,000 to 100,000 psi), the tendency for melting to occur during this energy discharge phase is reduced to a minimum. The increased pressure and localized temperature rise also contribute towards increased diffusion at and around the interfacial regions of the joint. This latter mechanism is called "stress-induced diffusion" and is caused by super-heating the material to high temperature levels in the solid state under pressure.

One question that arises in proposing this HDW metallurgical joining mechanism is whether a typical metal alloy lattice can accommodate the oxygen created during disassociation without producing porosity and other detrimental metallurgical defects. Since most alloys can safely absorb 100 to 200 ppm of oxygen atoms without producing porosity, the angstrom thick oxide layers on typical metal surfaces produce far less disassociated gas and are thus safely absorbed by the substrate.

Both the metallographic and electron beam microprobe analyses did not indicate the presence of oxides within the HDW joined regions of the similar and dissimilar alloy couples examined during this investigation. The above proposed mechanisms for HDW joining interface characteristics are offered as an explanation for the absence of oxide phases in the weld region.

Another point worth mentioning is the role of carbon in the ferrous alloy systems. The oxidation of carbon proceeds according to the following reaction:

$$C(s) + {}^1/_2O_2(g) = CO(g) \qquad (2)$$

Since the oxidation of carbon increases in negative, free energy of formation magnitude as the temperature increases (i.e., carbon monoxide becomes more stable), the ability of this element to reduce a metallic oxide at reduced temperatures is enhanced. Consider the formation of a simple iron oxide by the reaction:

$$Fe(s) + {}^1/_2O_2(g) = FeO(s) \qquad (3)$$

The subtraction of reaction (3) from reaction (2) produces:

$$FeO(s) + C(s) = Fe(s) + CO(g) \qquad (4)$$

i.e., the reduction of FeO(s) by C(s) to yield free iron and carbon monoxide. At ambient room termperature the resultant change in standard free energy of the reaction (4), i.e., $\Delta F^\circ_{(4)}$, is equal to $\Delta F^\circ_{(2)} - \Delta F^\circ_{(3)}$ and is a large, positive number. As the reaction temperature increases, $\Delta F^\circ_{(2)}$ tends to decrease in negative value, thus, causing $\Delta F^\circ_{(4)}$ to approach zero and become negative at temperatures below the melting point of ferrous alloys.

In practice, therefore, the presence of carbon and/or a similar or dissimilar ferrous alloy couple favors oxide disassociation and enhances the HDW joining. Also, there is sufficient carbon present to react with the surface iron oxides so that complete oxide disassociation can be accomplished at lower than normal weld temperatures. Consequently, the tendency for metastable, microstructural constituents to form is greatly reduced. Evidence of this latter effect can be observed in the photomicrographs of the ferrous alloy couples of this paper.

Conclusions

The results of this investigation indicate that the pulsed, high pressure joining process called hydro-dynamic welding can successfully weld various similar and dissimilar, ferrous and non-ferrous alloy couples. HDW produces optimum metallurgical features and minimal microstructural damage in either the base metal alloys or in the joined sections. The significant metallographic, microhardness and electron beam microprobe analysis results suggest the metallurgical joining mechanism for hydro-dynamic welding is as follows:

1. The short heating cycle results in a thin oxide skin buildup at the interface.

2. The localized pressure wave produced by the "self pinch" phenomenon seals the interface and reduction of the metal oxide commences in the joining region.

3. The lagging thermal spike created by the pressure pulse destroys the interfacial oxide and further promotes diffusion across the boundary, thus creating the hydro-dynamic welded joint.

References

1. "A Program for the Evaluation of a New Pipe Welding Method," Technical Report for the Portsmouth Naval Shipyard on work done under Contract NI02-79543(X), (1965).

2. Morin, T. J., Peacock, G. R., and Zotos, J., "Tubular Steel Welding Via a Shock Wave Technique," *Transactions*, American Foundrymen's Society, (1967).

3. Morin, T. J., Peacock, G. R., and Zotos, J., "Hydro-Dynamic Welding—A Major Breakthrough in Tubular Joining," WELDING JOURNAL, 47 (2), 114 to 117 (1968).

4. Morin, T. J., Whitehead, R. J., and Zotos, J., "Hydro-Dynamic Welding of Steel Tubes to Ferrous and Nonferrous Alloys," *Transactions*, American Foundrymen's Society, (1968).

5. Berardi, M. P., Peacock, G. R., Morin, T. J., and Zotos, J., "A New Concept in Joining Technology—HDW," American Society of Tool and Manufacturing Engineers, Paper AD-69-133, (May 1969).

6. Berardi, M. P., "Weld Tubing with Magnetic Shock Waves and Induction Heating," *Welding Design and Fabrication*, Vol. 42, No. 9, Pgs. 66-67, (September 1969).

7. Morin, T. J., and Zotos, J., "Welding Cast Iron to Steel Comes of Age," *Foundry*, Vol. 97, No. 12, Pgs. 119-127, (December 1969).

8. "Electron Beam Microanalysis of Hydro-Dynamic Welds," Advanced Metals Research Corporation, Special Report for Industrial Magnetics, Inc., (February 1970).

9. "Electron Beam Microanalysis of Hydro-Dynamic Welded Al-Cu and Zincated Al-Cu Tubing," Advanced Metals Research Corporation, Special Report for Industrial Magnetics, Inc., (March 1970).